Acta Crystallographica Section D
Biological Crystallography
ISSN 0907-4449

Structure of the minor pseudopilin XcpW from the *Pseudomonas aeruginosa* type II secretion system

Laura P. Franz,[a] Badreddine Douzi,[b,c] Eric Durand,[d] David H. Dyer,[a] Romé Voulhoux[d]* and Katrina T. Forest[a]*

[a]Department of Bacteriology, University of Wisconsin-Madison, Madison, WI 53706, USA, [b]Architecture et Fonction des Macromolecules Biologiques (AFMB–UMR6098), CNRS and Universités d'Aix-Marseille I and II, 13288 Marseille CEDEX 9, France, [c]Laboratoire des Maladies Transmissibles et Substances Biologiquement Actives (LR99ES27), Faculté de Pharmacie, TU-5000 Monastir, Tunisia, and [d]Laboratoire d'Ingénierie des Systèmes Macromoléculaires (LISM–UPR 9027), CNRS, Université de la Méditerranée, Institut de Microbiologie de la Méditerranée, 13402 Marseille CEDEX 20, France

Correspondence e-mail: voulhoux@ifr88.cnrs-mrs.fr, forest@bact.wisc.edu

Received 6 September 2010
Accepted 11 December 2010

PDB Reference: XcpW, 3nje.

Pseudomonas aeruginosa utilizes the type II secretion machinery to transport virulence factors through the outer membrane into the extracellular space. Five proteins in the type II secretion system share sequence homology with pilin subunits of type IV pili and are called the pseudopilins. The major pseudopilin $XcpT_G$ assembles into an intraperiplasmic pilus and is thought to act in a piston-like manner to push substrates through an outer membrane secretin. The other four minor pseudopilins, $XcpU_H$, $XcpV_I$, $XcpW_J$ and $XcpX_K$, play less well defined roles in pseudopilus formation. It was recently discovered that these four minor pseudopilins form a quaternary complex that is presumed to initiate the formation of the pseudopilus and to localize to its tip. Here, the structure of $XcpW_J$ was refined to 1.85 Å resolution. The structure revealed the type IVa pilin fold with an embellished variable antiparallel β-sheet as also found in the $XcpW_J$ homologue enterotoxigenic *Escherichia coli* $GspJ_W$ and the $XcpU_H$ homologue *Vibrio cholerae* $EpsU_H$. It is proposed that the exposed surface of this sheet may cradle the long N-terminal α1 helix of another pseudopilin. The final 31 amino acids of the $XcpW_J$ structure are instrinsically disordered. Deletion of this unstructured region of $XcpW_J$ did not prevent type II secretion *in vivo*.

1. Introduction

Many Gram-negative bacteria utilize the type II secretion system (T2SS) to secrete virulence factors. *Pseudomonas aeruginosa* uses its T2SS to secrete exotoxin A, phospholipase C, elastase, alkaline phosphatase and other substrates (Filloux, 2004). These exoproteins are translocated across the inner membrane *via* the Sec or twin-arginine translocation pathway followed by export across the outer membrane into the extracellular milieu *via* the T2SS (Pugsley, 1993; Voulhoux *et al.*, 2001).

P. aeruginosa uses 12 gene products, $XcpA_O$ and $XcpP_C$–Z_M, to form the T2SS machinery commonly termed the secreton (Tommassen *et al.*, 1992). Five *xcp* gene products in *P. aeruginosa* contain short N-terminal leader peptides with sequence homology to subunits of type IV pili and are therefore referred to as pseudopilins (Peabody *et al.*, 2003). These are $XcpT_G$, $XcpU_H$, $XcpV_I$, $XcpW_J$ and $XcpX_K$ (where the subscripts reference the T2SS protein names in the non-*Pseudomonas* T2SS; for example, in $XcpW_J$ the J refers to GspJ). This leader sequence on type IV pilins and T2S pseudopilins is removed by the prepilin peptidase $XcpA_O$, which cleaves between a conserved glycine at position −1 and a hydrophobic residue (often phenylalanine) at position +1.

$XcpA_O$ is known as PilD in the context of type IV pilus assembly (Nunn & Lory, 1993).

The major pseudopilin $XcpT_G$ is hypothesized to form an intraperiplasmic pilus, which acts as a piston to push substrates through the secretin $XcpQ_D$, the outer membrane pore (Filloux *et al.*, 1998). The energy for this process is generated by an inner membrane platform composed of $XcpR_E$, $XcpS_F$, $XcpY_L$ and $XcpZ_M$ (Filloux, 2004). The four low-abundance or minor pseudopilins $XcpU_H$, $XcpV_I$, $XcpW_J$ and $XcpX_K$ are believed to have accessory roles in T2S pseudopilus formation (Filloux *et al.*, 1998).

All five pseudopilins are essential for secretion, although the precise roles of the minor pseudopilins are still being investigated. The overproduction of $XcpT_G$ leads to a hyperpseudopilus that extends past the outer membrane. In contrast to the requirement for all four minor pseudopilins for T2S, only $XcpV_I$ is mandatory for the formation of the hyperpseudopilus (Durand *et al.*, 2005). The length of the hyperpseudopilus is controlled by the availability of $XcpX_K$ (Durand *et al.*, 2005). It has recently been shown in a systematic protein–protein interaction study that the four *P. aeruginosa* minor pseudopilins $XcpU_H$, $XcpW_J$, $XcpV_I$ and $XcpX_K$ are able to form a quaternary complex that is proposed to be at the tip of the $XcpT_G$-containing pseudopilus (Douzi *et al.*, 2009). Three of the four enterotoxigenic *Escherichia coli* (ETEC) T2SS homologues were also found to form a complex consisting of the minor pseudopilins $GspI_V$, $GspJ_W$ and $GspK_X$ (Korotkov & Hol, 2008). $GspK_X$ occupies the pinnacle position and is the largest; thus, the length-control function of $XcpX_K$ is possibly a consequence of its hindrance of the growth of the pseudopilus through the limiting opening in the outer membrane secretin (Korotkov & Hol, 2008).

In the present study, we analyzed one of the least well understood of the pseudopilins, $XcpW_J$. We expressed, purified and crystallized $XcpW_J$ and refined its structure to 1.85 Å resolution. The structure highlighted a region of intrinsic disorder that we interrogated by mutational analysis and provided a general testable model for the structural interaction of the T2SS minor pseudopilins with one another and with the major pseudopilin $XcpT_G$.

2. Materials and methods

2.1. Overexpression and purification of *P. aeruginosa* $XcpW_J$

The *xcpW*$_J$ plasmid, pETG-20A-W_J, was constructed by cloning the coding region for the soluble periplasmic domain of $XcpW_J$ (residues 22–231, lacking the N-terminal transmembrane helix; Fig. 1) into the Gateway (Invitrogen) pETG-20A vector as described previously (Douzi *et al.*, 2009). The expressed gene product includes an N-terminal thioredoxin followed by a six-residue histidine tag, nine amino acids encoded by the *att*B1 site, a second histidine tag, a tobacco etch virus (TEV) protease cleavage site and the soluble domain of $XcpW_J$ beginning with Arg22.

For each protein preparation, a fresh transformant of pETG-20A-W_J in *Escherichia coli* strain BL21 (DE3) pLysS (Promega) was inoculated into 100 ml Luria–Bertani (LB) medium containing 100 mg l^{-1} ampicillin and 34 mg l^{-1} chloramphenicol ($LB^{amp,chl}$). 25 ml aliquots of cultures grown overnight with shaking at 310 K were diluted into 1 l $LB^{amp,chl}$ and shaken at 310 K until the OD_{600} reached 0.4, at which point the temperature was lowered to 291 K. When the OD_{600} reached 0.6, *xcpW* expression was induced with 1 m*M* IPTG and growth continued overnight at 291 K. Cells were harvested by centrifugation at 9000*g* for 20 min at 279 K. The cell pellet was plunged into liquid nitrogen and stored at 193 K. 7 g thawed cell pellet was homogenized in 35 ml 50 m*M* imida-

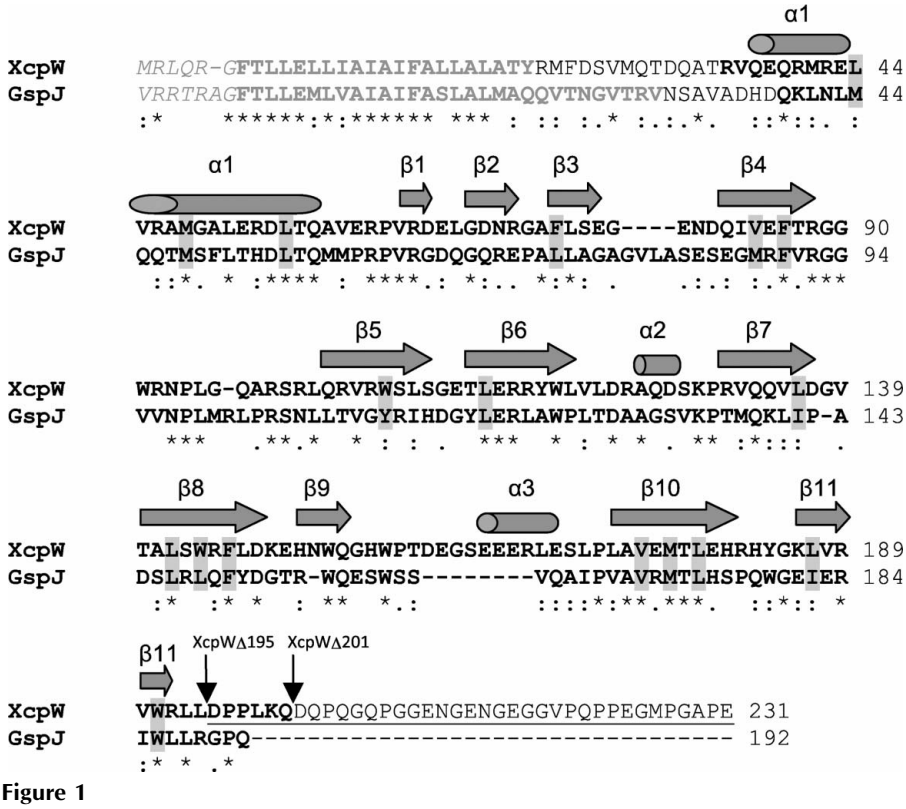

Figure 1
Sequence of *P. aeruginosa* $XcpW_J$. The primary sequence of $XcpW_J$ includes leader-peptide (grey italics) and transmembrane-helix residues that were removed for soluble expression (grey bold), unobserved residues (regular text), amino acids creating the conserved and symmetric hydrophobic core (grey shading), α-helices and β-strands in the $XcpW_J$ structure (cylinders and arrows, respectively) and the starting points for C-terminal deletions (black arrows and underlining). Following convention, numbering begins at the first residue of the mature protein (Phe +1); thus, the highly conserved glycine preceding the cleavage position is Gly −1. The sequence of $GspJ_W$ is 36% identical to that of $XcpW_J$ (asterisks and colons indicate identical and similar residues, respectively).

zole, 1× phosphate-buffered saline (PBS) and 250 U Benzonase Nuclease (Novagen). Cells were broken by two passes through a French press at 6.9 MPa and clarified by centrifugation at 58 500*g* for 30 min at 283 K. The supernatant was loaded onto a HisTrap FF 5 ml nickel-affinity resin column (Amersham Biosciences) equilibrated with 50 m*M* imidazole in PBS on an ÄKTAprime FPLC system. Following a wash with 30 column volumes, elution occurred during a gradient from 50 to 500 m*M* imidazole in PBS.

TEV protease was added to the purified fusion protein (32 µg ml^{-1} final concentration). During overnight cleavage, the protein was dialyzed into 50 m*M* HEPES pH 7.5 plus 3 m*M* β-mercaptoethanol (BME) at 277 K. The cleaved XcpW$_J$ was then loaded onto a nickel column equilibrated in 50 m*M* HEPES pH 7.5, which bound the (histidine-tagged) TEV protease and uncut protein. Flowthrough fractions that contained cleaved XcpW$_J$ based on SDS–PAGE analysis were concentrated using a 3000 molecular-weight cutoff concentrator (Millipore) and loaded onto a Superdex 75 (Amersham Biosciences) sizing column for further purification. Purified XcpW$_J$ was dialyzed overnight in 25 m*M* Tris pH 7.4. All protein samples were assessed for heterogeneity using dynamic light scattering. The polydispersity was generally around 25%.

2.2. Crystallization conditions

Initial XcpW$_J$ crystals were obtained using a sparse-matrix screen (JCSG, Qiagen). The crystals were grown at room temperature by vapour diffusion using the hanging-drop method (McPherson, 1982). The drops consisted of 1.5 µl protein solution at 17 mg ml^{-1} and 1.5 µl reservoir solution. For optimized crystals, the reservoir solution was 0.1 *M* HEPES pH 7.5, 15 m*M* KCl, 7.5% PEG 8000 and 0.1 *M* ATP (from 1 *M* stock dissolved in 25 m*M* Tris pH 8.0). The crystals grown with the ATP additive were approximately 0.2 mm in size and tear-drop-shaped. The crystals were cryopreserved in mother liquor containing 30% ethylene glycol.

Crystals were harvested for mass-spectrometric analysis in several steps. Firstly, a drop containing needle-like XcpW$_J$ crystals was transferred to a fresh glass cover slip. Mother liquor was slowly wicked from the crystals using absorbant paper. The crystals were resuspended in equilibrated mother liquor from the reservoir and this was also wicked away. The crystals were subsequently washed twice in 25 m*M* Tris–HCl pH 8.0 and then transferred into 25 µl filtered ddH_2O. This sample was analyzed for proteolysis of XcpW$_J$ by matrix-assisted laser desorption/ionization mass spectrometry.

2.3. Data collection, processing and refinement

A 1.85 Å resolution native data set was collected on beamline 21-ID-G at the Argonne National Laboratory's Advanced Photon Source (APS) using a MAR 300 CCD detector. The crystals belonged to space group $P2_1$, with two monomers in the asymmetric unit. The diffraction data were integrated, scaled and merged using *HKL*-2000 (Otwinowski & Minor, 1997). The structure was solved by molecular replacement with *Phaser* (McCoy *et al.*, 2007) using GspJ$_W$ (PDB entry 3ci0, chain *J*; Korotkov & Hol, 2008) as a model. The XcpW$_J$ structure was built using *Auto-Rickshaw* (Panjikar *et al.*, 2005) with manual fitting in *Coot* (Emsley & Cowtan, 2004). The large loop region connecting β4 and β5 of XcpW$_J$ could be traced in chain *B* (and was confirmed through the use of omit maps), but could not be fitted in chain *A* owing to poor electron density. The final structure was refined to 1.85 Å resolution using *REFMAC* v.5.5.0072. Translation, libration and screw-rotation displacement (TLS) groups that were defined by the *TLSMD* server (Painter & Merritt, 2006) were also used in the refinement process. The final overall R_{work} and R_{free} were 19.6% and 23.0%, respectively, and the XcpW$_J$ structure has 94.2% of residues in favoured regions of the Ramachandran plot, with no outliers (Table 1).

Structure factors and coordinates have been deposited in the Protein Data Bank with code 3nje.

Table 1
Crystallographic data collection and refinement of XcpW$_J$.

Values in parentheses are for the highest resolution shell.

Data collection	
Beamline	APS 21-ID-G
Wavelength (Å)	0.97856
Space group	$P2_1$
Unit-cell parameters (Å, °)	a = 39.7, b = 82.9, c = 57.8, $\alpha = \gamma$ = 90.0, β = 105.4
Resolution (Å)	25.0–1.85 (1.88–1.85)
Unique reflections	30798
Multiplicity	5.2 (5.1)
R_{merge}†	0.054 (0.394)
Completeness (%)	99.8 (99.9)
Average $I/\sigma(I)$	35.6 (3.6)
Refinement	
Molecules per asymmetric unit	2
No. of protein atoms	2871
No. of solvent atoms	193
R_{work}/R_{free}	0.196/0.230 (0.224/0.254)
Wilson B (Å^2)	22.8
Average B overall (Å^2)	19.9
R.m.s.d.	
Bond lengths (Å)	0.010
Bond angles (°)	1.240
Solvent content (%)	45.7
E.s.u.‡ (Å)	0.086
Ramachandran values	
Preferred regions (%)	94.2
Allowed regions (%)	5.8

† $R_{merge} = \sum_{hkl}\sum_i |I_i(hkl) - \langle I(hkl)\rangle| / \sum_{hkl}\sum_i I_i(hkl)$. ‡ Standard uncertainty of positional parameters based on maximum likelihood.

2.4. Construction of *xcp*W$_J$ mutants

The *xcpW*$_J$ alleles encoding wild-type XcpW$_J$ (XcpW$_J$wt), XcpW$_J$Δ195 and XcpW$_J$Δ201 (Fig. 1) were generated by PCR using the following oligonucleotides: XcpW$_J$up (5′-ATAGGATCCGCGCCGCGGCGCGCCTCGTCGGTTTCCTCG-3′) and XcpW$_J$down (5′-ATAAAGCTTCGACGCCGTTCTGCCCGCGCCTCATTCCGG-3′) for XcpW$_J$wt, XcpW$_J$up and XcpW$_J$Δ195down (5′-ATAAAGCTTTCAGAGCAGACGCCAGACGCGCACCAGCTTG-3′) for XcpW$_J$Δ195 and XcpW$_J$up and XcpW$_J$Δ201down (5′-ATAAAGCTTTCACTGCTTGAGCGGCGGATCGAGCAGACGC-3′) for

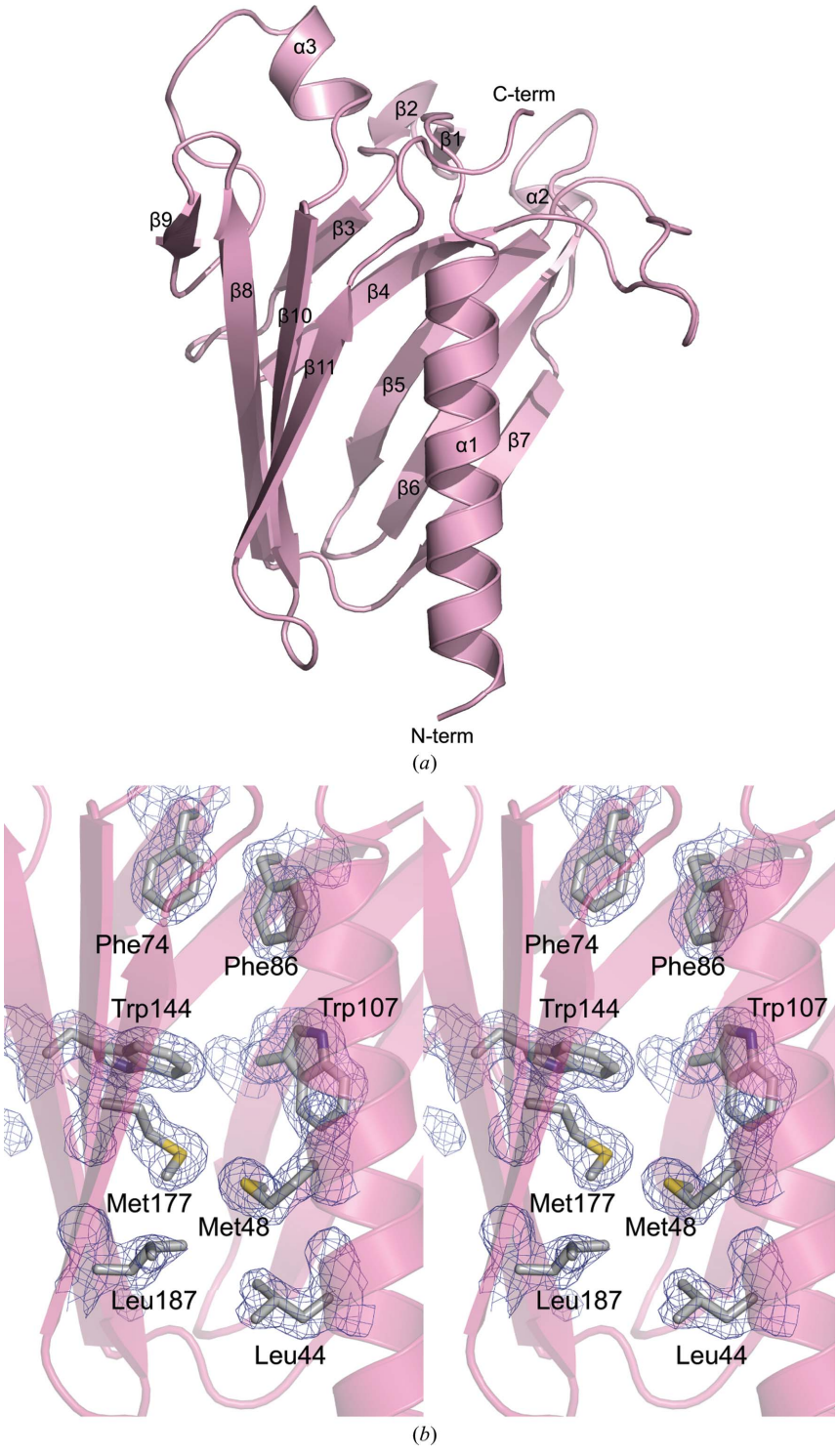

Figure 2
Structural features of XcpW$_J$. (*a*) XcpW$_J$ (ribbon representation with α-helices and β-strands indicated to highlight topology) displays the type IVa pilin fold consisting of a conserved N-terminal α1 packed against the C-terminal antiparallel β-sheet (β9–β8–β10–β11). α1 is flanked on the opposite side by a second antiparallel β-sheet (β3–β4–β5–β6–β7). (*b*) Eight of the 17 residues making up the hydrophobic core are shown in stereoview. Phe74 and Phe86 are two of the three phenylalanine side chains that form the canopy of the hydrophobic core. Trp144 and Trp107 are two of the three residues that create the tryptophan ring in the protein core. Met177, Met48, Leu187 and Leu44 portray the duplication that is seen throughout the hydrophobic core of XcpW$_J$ and GspJ$_W$.

XcpW$_J$Δ201. The resulting DNA fragments were cloned into the pCR2.1 vector (Invitrogen) and sequenced. These fragments were further digested with *Xba*I–*Sac*I restriction enzymes and subcloned into the arabinose-inducible host-range vector pJN105 (Newman & Fuqua, 1999), leading to plasmids pXcpW$_J$, pXcpW$_J$Δ195 and pXcpW$_J$Δ201. Recombinant plasmids were introduced into the wild-type *P. aeruginosa* strain PA01 or its Δ*xcp*W$_J$ derivative using the conjugative properties of pRK2013 (Figurski & Helinski, 1979). Transconjugants were selected on *Pseudomonas* isolation agar (Difco) supplemented with 50 µg ml^{-1} gentamicin (Gm^{50}).

2.5. Analysis of *xcp*W$_J$ mutants

Stable accumulation of the truncated forms of XcpW$_J$ was tested in *P. aeruginosa*. Bacteria were grown at 303 K in TSB liquid medium (Difco) overnight with the addition of 2% L-arabinose (Ara). After overnight growth, the cells were collected and resuspended in SDS–PAGE sample buffer. Protein samples were analyzed as described in Voulhoux *et al.* (2001) on a 15% SDS–polyacrylamide gel (Bio-Rad III) followed by Western blotting using anti-XcpW$_J$ primary antibody (1:5000; Douzi *et al.*, 2009).

Secreted protein profiles were analyzed from *P. aeruginosa* strains grown as described above. Cells and extracellular medium were separated by centrifugation; proteins contained in the supernatants were precipitated by adding trichloroacetic acid [15%(*w*/*v*) final concentration] and incubating for 2 h at 277 K. Samples were subsequently centrifuged (30 min at 15 000*g*), the pellets were washed with 90%(*v*/*v*) acetone, resuspended in SDS–PAGE sample buffer and analyzed as described in Voulhoux *et al.* (2001) on a 12% SDS-polyacrylamide gel stained with Coomassie Blue.

For functional secretion assays, *P. aeruginosa* strains were grown overnight in liquid medium at 310 K. Culture samples were plated on (Gm^{50}, 2% Ara) plates. Protease secretion was tested on TSA (Difco) plates containing 1.5% dried milk, with the zone of clearing indicating the secretion of active protease. For the detection of lipase secretion, lipid agar plates were used. Lipid agar is a minimal medium containing olive oil as the sole carbon source (Kagami *et al.*, 1998).

3. Results and discussion

3.1. The structure of XcpW$_J$

We have solved and refined the crystal structure of a soluble construct of XcpW$_J$ (Fig. 1), one of the minor pseudopilins in the *P. aeruginosa* T2SS. The electron density for the XcpW$_J$ structure was clearly defined from Arg35 through Trp91 in chain *A* and from Gln37 through Leu102 in chain *B*. Residues Gln103–Gln200 had well defined electron density for both monomers in the asymmetric unit. The remaining 31 residues at the C-terminus of XcpW$_J$ could not be modelled and therefore are not included in the final coordinates. Mass spectrometry of washed crystals indicated that 30 of these C-terminal amino acids (along with eight N-terminal amino acids) had been cleaved during crystallization (data not shown). This sequence contains 50% proline or glycine residues (Fig. 1), which are likely to be the cause of intrinsic disorder in this region and may have contributed to the proteolytic susceptibility (Radivojac *et al.*, 2004).

The XcpW$_J$ structure revealed the typical type IVa pilin fold distinguished by a long N-terminal α-helix that packs against an antiparallel β-sheet (β9–β8–β10–β11; Fig. 2*a*). β9 makes only four nonstandard main-chain hydrogen bonds with β8 main-chain atoms, while β8–β10–β11 form the more canonical conserved sheet. XcpW$_J$ contains a complex domain inserted between these two conserved structural elements consisting of a five-stranded antiparallel β-sheet (β3–β4–β5–β6–β7). Several long excursions between the strands give XcpW$_J$ its distinctive surface shape. Such an insertion in the structurally variable position between α1 and the conserved β-sheet (given the moniker '$\alpha\beta$ loop' in type IVa pilins; Craig *et al.*, 2003) is also seen in the ETEC GspJ$_W$, *V. vulnificus* EpsJ and *V. cholerae* EpsH$_U$ minor pseudopilin structures (Korotkov & Hol, 2008; Yanez *et al.*, 2008*a*,*b*), although the sheet topology differs between J$_W$ and H$_U$ pseudopilins. This region has been called the 'variable sheet' to distinguish it from the 'conserved sheet' seen in every type IV pilin and pseudopilin structure solved to date.

An intriguing feature of the XcpW$_J$ structure is an internally symmetric hydrophobic core (Fig. 2*b*). The residues that make up this symmetry are Leu44 on the N-terminal α-helix and Leu187 on β11, Leu55 on the N-terminal α-helix and Leu179 on β10, Leu114 on β6 and Leu142 on β8, Met48 on the N-terminal α-helix and Met177 on β10, and Val84 on β4 and Val175 on β10. There are also three phenylalanine residues that form a canopy over the hydrophobic core. These are Phe74 on β3, Phe86 on β4 and Phe146 on β8. Along with these hydrophobic residues there are three tryptophan residues in a ring within the core: Trp107 on β5, Trp144 on β8 and Trp191 on β11. These internally symmetric hydrophobic residues are conserved in ETEC GspJ$_W$ (Fig. 1). It has been shown recently that many, if not all, major T2SS pseudopilins rely on calcium for stability, unlike type IVa pilin subunits, which contain disulfide bridges (Korotkov *et al.*, 2009). The well packed interior and lack of metal ions in the XcpW$_J$ and GspJ$_W$ structures lead us to believe these pseudopilins rely completely on their hydrophobic cores for stability.

3.2. Features of the variable sheet

The variable sheet of XcpW$_J$ is framed by small structural elements that create a polar gulley on the surface of the monomer (Fig. 3). 'Overhang 1' is formed by α2, 'overhang 2' is the β1–β2 hairpin, the 'back door' is the α3 helix between β9 and β10 and the 'floor' is the loop between β3 and β4. Three of these are structurally distinct between XcpW$_J$ and GspJ$_W$, which otherwise have very similar folds as evidenced by their r.m.s.d. of 1.2 Å over the 701 most structurally similar atoms (Fig. 3; DeLano, 2002). α2 of XcpW$_J$ is absent in GpsJ$_W$, α3 replaces a loop in GspJ$_W$ and the minimal 'floor' in XcpW$_J$ is a short helix in GspJ$_W$. Nine of the 11 negatively charged residues found in XcpW$_J$ but not GspJ$_W$ (Glu66, Asp69, Glu79, Asp81, Asp137, Asp160, Glu161, Glu165 and Glu169; Fig. 1) are located within the loops that surround the variable sheet. Altering these acidic residues to uncharged residues could define their importance in maintaining the Xcp quaternary complex stability or substrate recognition. In addition to these

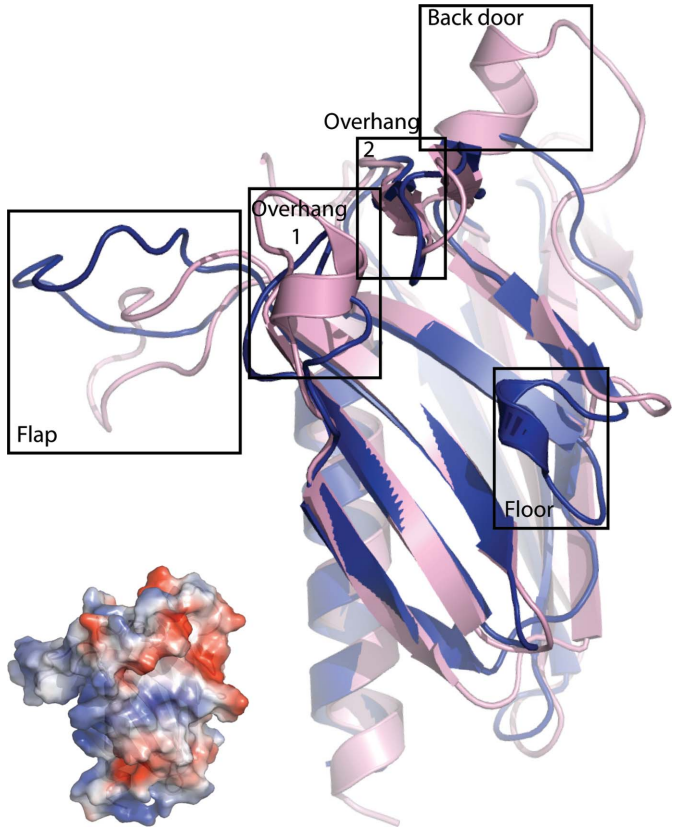

Figure 3
Elements of the variable sheet of XcpW$_J$ and ETEC GspJ$_W$. The strong structural similarity between XcpW$_J$ (pink) and GspJ$_W$ (blue) includes the pilin fold and variable β-sheet. Notable differences between XcpW$_J$ and GspJ$_W$ include α2 (overhang 1), the α3 helix between β9 and β10 in XcpW$_J$ (back door), the small α2 helix in GspJ$_W$ that is lacking between β3 and β4 of the XcpW$_J$ (floor) and the different orientation of the loop between XcpW$_J$ β4 and β5 (flap). The exposed surface of the variable sheet is polar, as seen in the electrostatic potential of XcpW$_J$ estimated within *PyMOL* (DeLano, 2002; insert on lower left in identical orientation to the cartoon, with red negative and blue positive regions ranging from −76 to +76 kT/e).

structural distinctions around the variable sheet, the large flap between β4 and β5 of XcpW$_J$ is in a different conformation to that in the GspJ$_W$ structure (Fig. 3).

Why does XcpW$_J$ have a variable β-sheet? In every major (pseudo)pilin the conserved β-sheet cradles the long N-terminal α1 helix and the repetition of these two structural elements over tens to hundreds of subunits allows filament formation. We speculate that the variable second sheet in XcpW$_J$ may create a Janus-faced exterior surface for the similar packing of the exposed side of a second pseudopilin α1 helix. This helix could belong to another minor pseudopilin such as XcpU$_H$ or the major pseudopilin XcpT$_G$ itself. In this regard, it is interesting to note that the XcpU$_H$ and XcpT$_G$ major helices are amphipathic, with a charged face that could potentially complement the polar surface of XcpW$_J$ (Fig. 3, inset). By extension, we suggest the same role for the variable sheet predicted for XcpU$_H$ based on its homology to EpsH$_U$ (Yanez *et al.*, 2008*b*). Such packing would interrupt the continuity of the pseudopilus helix and provide a mechanism both for XcpU$_H$–XcpW$_J$ interaction (Douzi *et al.*, 2009) and for the transition from the complex of pseudopilins to the repetitive downward assembly of XcpT$_G$.

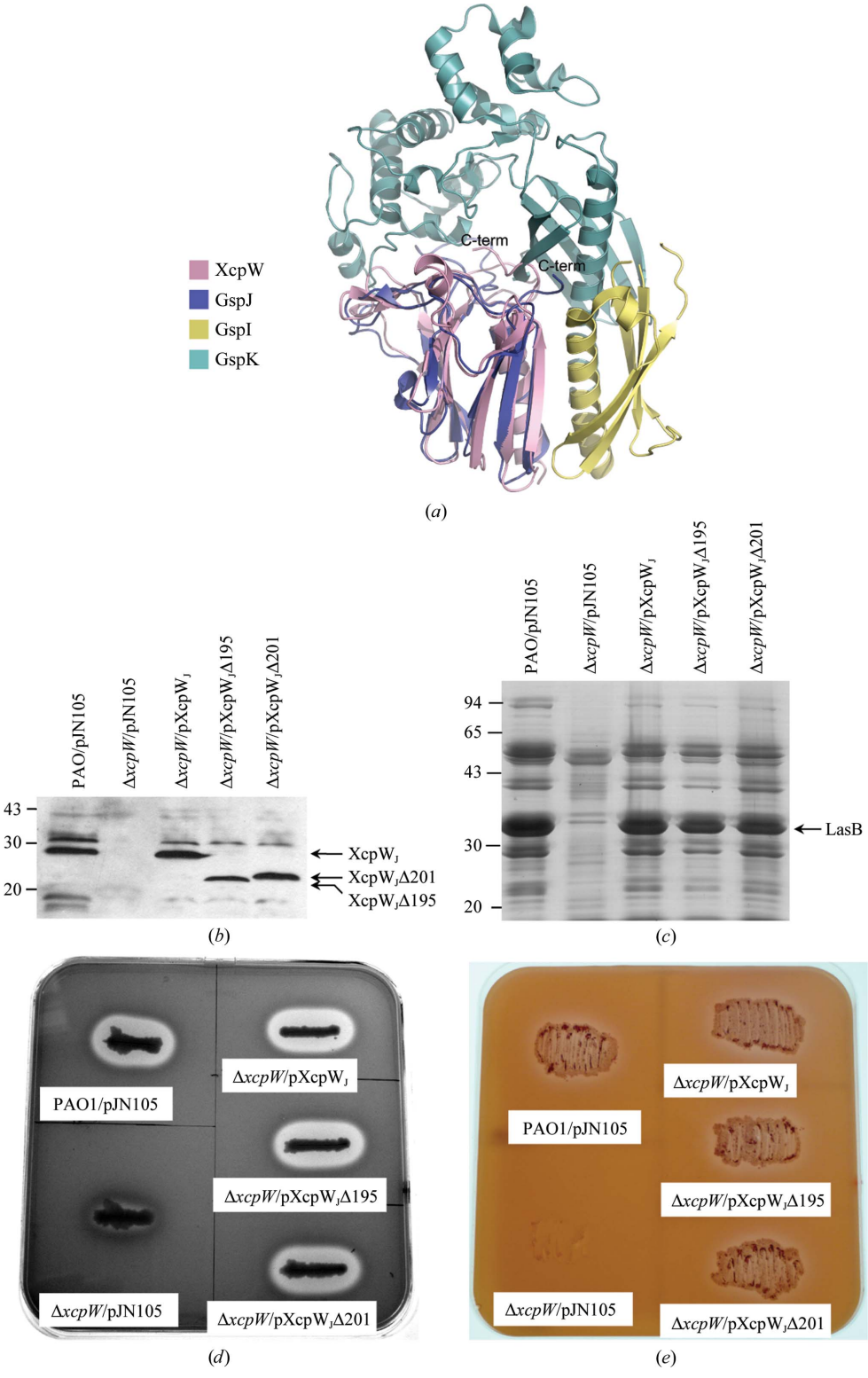

3.3. Functional interrogation of the C-terminal tail

The C-terminal end of XcpW$_J$ features a uniquely long extension among the GspJ$_W$ pseudopilins (Fig. 1). When XcpW$_J$ is

Figure 4
Analysis of the position and function of the C-terminal disordered region. (*a*) Structural alignment of XcpW$_J$ (pink) with the ETEC GspI$_V$ (yellow)–GspJ$_W$ (blue)–GspK$_X$ (cyan) complex suggests the disordered C-terminus of XcpW$_J$ could lie near or in the cleft between GspJ$_W$ and GspK$_X$. (*b*) XcpW$_J$Δ195 and XcpW$_J$Δ201 are produced in Δ*xcp*W$_J$ when carried on a plasmid and expressed from the arabinose-inducible promoter, as seen in this Western blot using anti-XcpW$_J$ serum against whole cell lysates. (*c*) Complementation of the Δ*xcp*W$_J$ mutant by either truncated *xcp*W$_J$ gene restored protein secretion to the extracellular medium. The major Xcp T2SS-dependent substrate elastase (LasB) is indicated in this Coomassie-stained SDS–polyacrylamide gel of culture supernatants. (*d*) Elastase and (*e*) lipase secretion on skim milk or lipid agar plates, respectively, is restored when the Δ*xcp*W$_J$ mutant is complemented by one of the two truncated forms of XcpW$_J$. The halo around the colony on the skim milk plate corresponds to milk degradation owing to elastase activity (*c*). The lipid agar plate contains a minimal medium on which only T2S-proficient strains grow (*d*).

structurally aligned with $GspJ_W$ in the $GspI_V$–$GspJ_W$–$GspK_X$ ternary complex (Korotkov & Hol, 2008) it appears that the C-terminal extension could lie within the groove between $GspK_X$ and $GspJ_W$ (Fig. 4*a*), suggesting that it might play a role in holding the minor pseudopilin complex together. Since it is difficult to predict the structural organization of this 31-amino-acid intrinsically disordered tail or any interaction that it may make with other minor pseudopilins or T2SS components, we created $XcpW_J$ variants missing 37 or 31 amino acids and tested their functionality *in vivo* (Figs. 4*b*–4*e*). Both truncated forms of $XcpW_J$, $XcpW_J\Delta195$ and $XcpW_J\Delta201$, were produced with their expected molecular weight (Fig. 4*b*). Both restored wild-type secretion profiles when used to complement an *xcp*W_J deletion strain (Fig. 4*c*). In addition, the extracellular activity of two T2SS-dependent substrates, elastase (Fig. 4*d*) and lipase (Fig. 4*e*), is restored with either truncated form of $XcpW_J$. Although we cannot rule out a subtle effect in recognition or chaperoning of a subset of the Xcp secretion substrates, these data uncover no obvious differences between full-length and C-terminally truncated $XcpW_J$. We conclude that the Pro/Gly-rich tail of $XcpW_J$ is not required for functional interaction with the rest of the Xcp secreton.

We can now also further interpret results from experiments on $XpsJ_W$, the $XcpW_J$ homolog from the *Xanthamonus campestris* T2SS. Kuo *et al.* (2005) found that the truncation of up to 14 amino acids from the C-terminus of $XpsJ_W$ had a less than twofold effect on the secretion of amylase from *X. campestris*, but removal of 17 or more amino acids impaired amylase secretion and proper cellular localization of $XpsJ_W$ (Kuo *et al.*, 2005). In light of our findings, it is notable that $XpsJ_W$ has an 11-amino-acid Pro/Gly-rich tail which seems to be dispensable in the amylase-secretion system, whereas the inactive truncations remove part of the last predicted β-strand in the conserved sheet.

Our physiological result that the Pro/Gly tail is not needed for T2S despite the juxtaposition of the tail of $XcpW_J$ with $XcpX_K$ in the structural model (Fig. 4*a*) is well correlated with the observation that the soluble construct of $XcpW_J$ interacts with soluble domains of $XcpU_H$ and $XcpV_I$ but not $XcpX_K$ (Douzi *et al.*, 2009). It may be that the *P. aeruginosa* $XcpW_J$–$XcpX_K$ interaction differs somewhat from that of the crystalline interaction of ETEC $GspJ_W$–$GspK_X$ (Fig. 3*a*; Korotkov *et al.*, 2009). Future mutational work should elucidate which regions of $XcpW_J$ are required for Xcp complex formation. Definitive identification of the disposition of each minor pseudopilin within the T2SS will await the structure determination of the $XcpU_H$–$XcpV_I$–$XcpW_J$–$XcpX_K$ quaternary complex.

This work was funded by the US National Institutes of Health (GM59721) and the French Agence Nationale de la Recherche (ANR-JC07-183230). Use of the Advanced Photon Source was supported by the US Department of Energy, Office of Science, Office of Basic Energy Sciences under Contract No. DE-AC02-06CH11357. Use of the LS-CAT Sector 21 was supported by the Michigan Economic Development Corporation and the Michigan Technology Tri-Corridor for the support of this research program (Grant 085P1000817).

References

Craig, L., Taylor, R. K., Pique, M. E., Adair, B. D., Arvai, A. S., Singh, M., Lloyd, S. J., Shin, D. S., Getzoff, E. D., Yeager, M., Forest, K. T. & Tainer, J. A. (2003). *Mol. Cell*, **11**, 1139–1150.
DeLano, W. L. (2002). *PyMOL.* http://www.pymol.org.
Douzi, B., Durand, E., Bernard, C., Alphonse, S., Cambillau, C., Filloux, A., Tegoni, M. & Voulhoux, R. (2009). *J. Biol. Chem.* **284**, 34580–34589.
Durand, E., Michel, G., Voulhoux, R., Kurner, J., Bernadac, A. & Filloux, A. (2005). *J. Biol. Chem.* **280**, 31378–31389.
Emsley, P. & Cowtan, K. (2004). *Acta Cryst.* D**60**, 2126–2132.
Figurski, D. H. & Helinski, D. R. (1979). *Proc. Natl Acad. Sci. USA*, **76**, 1648–1652.
Filloux, A. (2004). *Biochim. Biophys. Acta*, **1694**, 163–179.
Filloux, A., Michel, G. & Bally, M. (1998). *FEMS Microbiol. Rev.* **22**, 177–198.
Kagami, Y., Ratliff, M., Surber, M., Martinez, A. & Nunn, D. N. (1998). *Mol. Microbiol.* **27**, 221–233.
Korotkov, K. V., Gray, M. D., Kreger, A., Turley, S., Sandkvist, M. & Hol, W. G. (2009). *J. Biol. Chem.* **284**, 25466–25470.
Korotkov, K. V. & Hol, W. G. (2008). *Nature Struct. Mol. Biol.* **15**, 462–468.
Kuo, W.-W., Kuo, H.-W., Cheng, C.-C., Lai, H.-L. & Chen, L.-Y. (2005). *J. Biomed. Sci.* **12**, 587–599.
McCoy, A. J., Grosse-Kunstleve, R. W., Adams, P. D., Winn, M. D., Storoni, L. C. & Read, R. J. (2007). *J. Appl. Cryst.* **40**, 658–674.
McPherson, A. (1982). *The Preparation and Analysis of Protein Crystals.* New York: Wiley.
Newman, J. R. & Fuqua, C. (1999). *Gene*, **227**, 197–203.
Nunn, D. N. & Lory, S. (1993). *J. Bacteriol.* **175**, 4375–4382.
Otwinowski, Z. & Minor, W. (1997). *Methods Enzymol.* **276**, 307–326.
Painter, J. & Merritt, E. A. (2006). *Acta Cryst.* D**62**, 439–450.
Panjikar, S., Parthasarathy, V., Lamzin, V. S., Weiss, M. S. & Tucker, P. A. (2005). *Acta Cryst.* D**61**, 449–457.
Peabody, C. R., Chung, Y. J., Yen, M.-R., Vidal-Ingigliardi, D., Pugsley, A. P. & Saier, M. H. Jr (2003). *Microbiology*, **149**, 3051–3072.
Pugsley, A. P. (1993). *Microbiol. Rev.* **57**, 50–108.
Radivojac, P., Obradovic, Z., Smith, D. K., Zhu, G., Vucetic, S., Brown, C. J., Lawson, J. D. & Dunker, A. K. (2004). *Protein Sci.* **13**, 71–80.
Tommassen, J., Filloux, A., Bally, M., Murgier, M. & Lazdunski, A. (1992). *FEMS Microbiol. Rev.* **9**, 73–90.
Voulhoux, R., Ball, G., Ize, B., Vasil, M. L., Lazdunski, A., Wu, L.-F. & Filloux, A. (2001). *EMBO J.* **20**, 6735–6741.
Yanez, M. E., Korotkov, K. V., Abendroth, J. & Hol, W. G. (2008*a*). *J. Mol. Biol.* **375**, 471–486.
Yanez, M. E., Korotkov, K. V., Abendroth, J. & Hol, W. G. (2008*b*). *J. Mol. Biol.* **377**, 91–103.